Original article

Synthesis, in vitro and in silico screening of ethyl 2-(6-substituted benzo[d]thiazol-2-ylamino)-2-oxoacetates as protein-tyrosine phosphatase 1B inhibitors☆

Gabriel Navarrete-Vazquez [a,*], Marleth Ramírez-Martínez [a], Samuel Estrada-Soto [a], Carlos Nava-Zuazo [a], Paolo Paoli [b], Guido Camici [b], Jaime Escalante-García [c], José L. Medina-Franco [d], Fabian López-Vallejo [d], Rolffy Ortiz-Andrade [e]

[a] Facultad de Farmacia, Universidad Autónoma del Estado de Morelos, Av Universidad 1001, Chamilpa, Cuernavaca 62209, Morelos, Mexico
[b] Dipartimento di Scienze Biochimiche, Università degli Studi di Firenze, Firenze 50134, Italy
[c] Centro de Investigaciones Químicas, Universidad Autónoma del Estado de Morelos, Cuernavaca, Morelos 62209, Mexico
[d] Torrey Pines Institute for Molecular Studies, Port St. Lucie, FL 34987, USA
[e] Facultad de Química, Universidad Autónoma de Yucatán, Mérida, Yucatán 97000, Mexico

ARTICLE INFO

ABSTRACT

The ethyl 2-(6-substituted benzo[d]thiazol-2-ylamino)-2-oxoacetate derivatives (**OX 1–9**) were prepared using a one-step reaction. The in vitro inhibitory activity of the compounds against protein tyrosine phosphatase 1B (PTP-1B) was evaluated. Compounds **OX**-(**1**, **6** and **7**) were rapid reversible (mixed-type) inhibitors of PTP-1B with IC_{50} values in the low micro-molar range. The most active compounds **OX**-(**1**, **6** and **7**) were docked into the crystal structure of PTP-1B. Docking results indicate potential hydrogen bond interactions between the oxamate group in all compounds and the catalytic amino acid residues Arg221 and Ser216. The compounds were evaluated for their in vivo hypoglycemic activity, showing significant lowering of plasma glucose concentration in acute normoglycemic model and oral glucose tolerance test similarly at the effect exerted for hypoglycemic drug glibenclamide.

© 2012 Elsevier Masson SAS. All rights reserved.

1. Introduction

Diabetes mellitus is a chronic and progressive disease of metabolic deregulation characterized by insulin resistance in peripheral tissues (liver, muscle, and adipose), and impaired insulin secretion by the pancreas [1].

Type-2 diabetes and obesity are related with the deficiency in insulin receptor signaling and is supposed to be recovered by the inhibition of a certain protein-tyrosine phosphatases involved in the down-regulation of insulin receptor, which causes prolonged phosphorylation of the insulin receptor kinase [2–4]. The protein-tyrosine phosphatase 1B (PTP-1B) plays a key role in cellular signaling and in several human diseases, particularly diabetes and obesity [5]. This enzyme is a novel attractive therapeutic target for the treatment of diabetes [6]. Recently, our group reported a series of 2-arylsulfonylaminobenzothiazoles, which were weak inhibitors of PTP-1B (Fig. 1) [7].

However, compounds displayed appreciable in vivo activity in a non-insulin-dependent diabetes mellitus murine model, comparable to glibenclamide [7]. In order to find new class of compounds with hypoglycemic action, we report in this article the one-step synthesis of ethyl 2-(6-substituted benzo[d]thiazol-2-ylamino)-2-oxoacetate derivatives (**OX**-(**1–9**), Table 1), their in vitro inhibitory activity on the PTP-1B, molecular docking of the most active compounds as well as the in vivo hypoglycemic effect in normoglycemic rats.

2. Results and discussion

2.1. Chemistry

Compounds **OX**-**1** to **OX**-**8** were synthesized starting from 2-amino-6-substituted benzo[d]thiazole (**10–17**), via a coupling reaction with ethyl chlorooxoacetate (**18**), in the presence of triethylamine. Compound **OX**-**9** was prepared by catalytic reduction of compound **OX**-**8**. Title compounds were recovered with 44–98% yields (Table 1). Compounds were purified by recrystalization or by column chromatography. The chemical structures of the synthesized compounds were confirmed on the basis of their spectral data (NMR and mass spectra), and their purity ascertained

---

R= -CH$_3$: IC$_{50}$= 19.5 M, *Ki*: 7.1 M
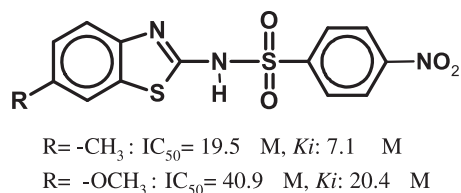R= -OCH$_3$: IC$_{50}$= 40.9 M, *Ki*: 20.4 M

Fig. 1. Structure of 2-arylsulfonylaminobenzothiazoles inhibitors of PTP-1B [7].

by microanalysis. Physical constants of the title compounds are shown in Table 1.

In the nuclear magnetic resonance spectra (^{1}H NMR; δ ppm), the signals of the respective protons of the compounds were verified on the basis of their chemical shifts, multiplicities, and coupling constants. The aromatic region of the ^{1}H NMR spectrum contained an ABX pattern signals ranging from δ 7.06–8.24 ppm (dd, J_m = 1.0–2.4; J_o = 7.5–8.8 Hz), 7.61–7.89 (d, J_o = 8.8 Hz), and 7.59–8.43 (d, J_m = 1.1–2.6 Hz) attributable to H-5, H-4, and H-7, of the benzothiazole-6-substituted structure, respectively. The signals for ethyl oxamate were found ranging from δ 3.80–4.32 ppm assignable to CH$_2$, and 1.20–1.34 attributable to CH$_3$.

2.2. In vitro PTP-1B inhibition assay

To test the ability of each compound to inhibit PTP-1B, aliquots of stock solutions (dissolved in DMSO to prepare 20 mM) were diluted with the assay buffer, containing 2.5 mM *p*-nitrophenyl phosphate (*p*-NPP), to the final concentration of 40 μM. Samples were incubated at 37 $^\circ$C, and the reactions were initiated by adding an appropriate enzyme aliquot. Fig. 2 shows that compounds **OX**-1, **OX**-6, and **OX**-7 strongly reduce the PTP-1B activity, whereas all other compounds showed weaker activity.

Taking into account the results of the above preliminary analyses, we performed additional assays on the most active compounds **OX**-1, **OX**-6, and **OX**-7 to explore the type of inhibition. Appropriate aliquots of PTP-1B were incubated in the presence of a 125-fold molar excess of inhibitor for 1 h at two differing temperature, 4 $^\circ$C and 37 $^\circ$C. Control experiments were performed adding DMSO instead of the inhibitor solution. After this interval time, the enzyme solutions were diluted 400-fold with the assay solution, and the residual enzyme activity was measured. The results, shown in the Fig. 3, demonstrate that the recovery of the enzyme activity is almost complete in all cases, suggesting that all **OX**-1, **OX**-6, and **OX**-7 act as reversible inhibitors.

To assess the ability of **OX**-1, **OX**-6, and **OX**-7 to behave as slow-binding inhibitors, we studied the PTP-1B catalyzed hydrolysis of *p*-
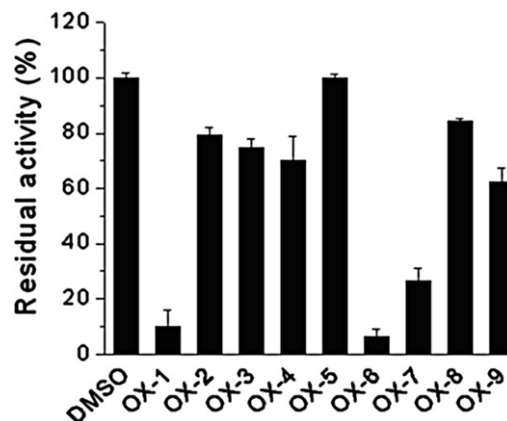

Fig. 2. Inhibition of PTP-1B activity by **OX**-(1–9) compounds. Inhibition assays were performed at 37 $^\circ$C and pH 7.0 at a fixed substrate final concentration (2.5 mM *p*-NPP), which is a value close to that of K_m for PTP-1B at pH 7.0. The final concentration of each compound in the reaction assay was 40 μM. Each assay (final volume 1 ml) was started with 0.16 μg of PTP-1B. Control experiment was carried out using DMSO. Each datum represents the means $\pm$ S.E.M. of four distinct assays. Residual activity, expressed as percentage, is defined as the ratio between enzyme activity measured in the presence of the inhibitor and that of the control.

nitrophenyl phosphate in the presence of different inhibitor concentrations, measuring the time-course of *p*-nitrophenol release at 400 nm. In all cases we found that initial rates decrease with increasing inhibitor concentrations, and curves maintain linear monophasic behaviors as time progresses, indicating that the rapid equilibrium conditions occur in the formation of enzyme–inhibitor complexes. Identical behavior was found pre-incubating PTP-1B with inhibitors for 30 min before the activity assay. Taken together our results suggest that both association and dissociation of inhibitors to the enzyme are fast events, excluding the hypothesis that these compounds are slow-binding inhibitors. To better evaluate the inhibitory power of these compounds, their IC$_{50}$ values were determined. Fig. 4 show the concentration–response plots by the most active compounds **OX**-1, **OX**-6, and **OX**-7. Table 2 summarizes the corresponding IC$_{50}$ values, which are in the low micro-molar range.

Thus, our assay system is operated under non-tight binding conditions in the case of each inhibitor examined since IC$_{50}$ is greater than 5-fold over enzyme concentration (10 nM in all assays) and the approximation that [inhibitor] free = [inhibitor] total is valid.
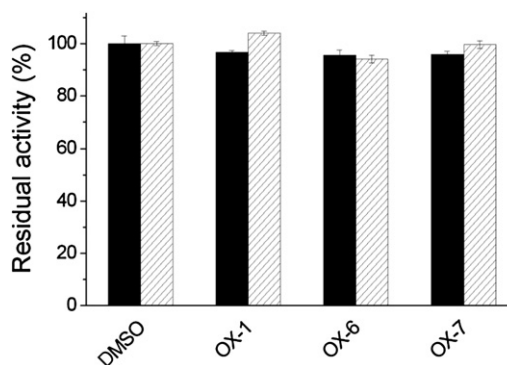
Table 1
Synthesis and physicochemical data for derivatives **OX**-(1–9).

Compd	R	MW	Mp ($^\circ$C)	Unoptimized yield (%)
OX-1	−CH$_3$	265	163–165	52
OX-2	−H	251	187–188	49
OX-3	−OCH$_3$	280	182–184	45
OX-4	−OCH$_2$CH$_3$	295	176–178	44
OX-5	−SO$_2$CH$_3$	329	209–212	98
OX-6	−Cl	285	218–221	47
OX-7	−F	269	214–215	63
OX-8	−NO$_2$	295	255(dec.)	80
OX-9	−NH$_2$	265	282 (dec.)	92

Fig. 3. Inhibition reversibility assay. Aliquots of PTP-1B were incubated in the presence of 100 μM of each compound for 1 h at 4 $^\circ$C (black bar) or 37 $^\circ$C (white bar). Then the enzyme was diluted 400-fold with the assay solution to measure the residual activity (37 $^\circ$C, 5 mM pNPP final concentration). Control experiments were carried out adding DMSO. All tests were performed in triplicate. The data represent the mean $\pm$ S.E.M.
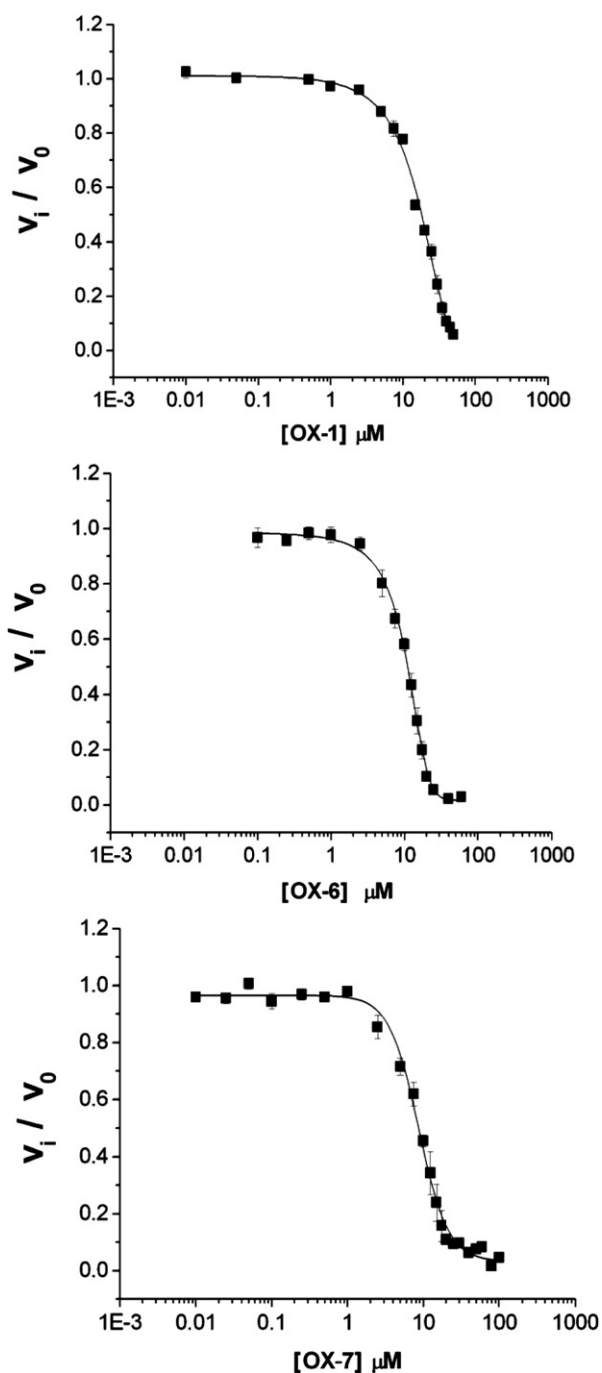
Fig. 4. The IC_{50} values were determined by plotting the relative activity of PTP-1B versus inhibitor concentration. For each inhibitor, 15–20 different inhibitor concentrations were used. All tests were performed in quadruplicate. The data represent the means ± S.E.M.

To verify if some compounds act as partial inhibitors, we measured the rate of PTP-1B-catalyzed hydrolysis of *p*-nitrophenyl phosphate at high substrate concentration (10-fold the K_m value of the enzyme) in the presence of increasing concentrations of each compound. The results obtained for **OX**-1, **OX**-6, and **OX**-7 are reported in Fig. 5. We can observe that, by increasing the inhibitor concentration, the hydrolysis rate is reduced near to zero, suggesting that the binding of inhibitor to enzyme produces an inactive EI complex.

To determine the kinetic mechanism of inhibition, we studied the dependence of enzyme main kinetic parameters (K_m and V_{max}) from the inhibitors concentration. For each compound, we measured the initial hydrolysis rate using height substrate final concentrations (0.5–40 mM range), in the presence of increasing concentrations of each compound (Fig. 6). Experimental data was analyzed by the double reciprocal plot method.

All reciprocal plots for **OX**-1, **OX**-6, and **OX**-7 show straight lines that intersect each other in the left panel demonstrating that they are mixed-type inhibitors. This is confirmed by the fact that increasing inhibitor concentration is accompanied by the increase of K_m values and the decrease of V_{max} (values Figs. 6–8).

To determine the K_i and the α values for the mixed-type inhibitors **OX**-1, **OX**-6, and **OX**-7 we considered the model represented in Scheme 1.

In this model, the inhibitor binds both the free enzyme, E, and the enzyme–substrate complex, ES. The EI has lower affinity for S than E ($\alpha > 1$), and ESI is non-productive. We calculated the value of K_i (mixed-type) by replotting the slope of the straight lines of the double reciprocal plot versus [I], using the following equation:

$$\text{slope} = \frac{K_m}{K_t \times V_{max}} \times [I] + \frac{K_m}{V_{max}}$$

The results are reported in Table 3.

2.3. Molecular docking of compounds **OX**-(*1*, *6* and *7*) with PTP-1B

In order to gain insight into the putative binding mode of the most active compounds with PTP-1B, these compounds were docked with a crystallographic structure of human PTP-1B using AutoDock4 [11]. The crystallographic structure was obtained from the Protein Data Bank (PDB), accession code 1C83 [8]. PTP-1B is co-crystallized with 6-(oxalyl-amino)-1*H*-indole-5-carboxilic acid which shows an extensive hydrogen bond network with residues in the catalytic site. The catalytic residues, Arg221 and Asp181, play a key role in the binding mode of the co-crystallized ligand (Fig. 9).
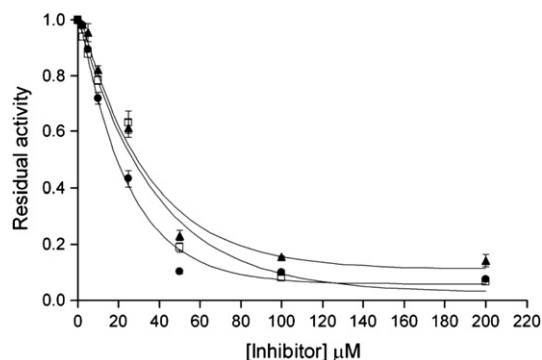
Fig. 5. The residual enzyme activity was measured at 37 °C and pH 7.0 using 25 mM pNPP as substrate. The inhibitors concentrations used were: 2.5, 5.0, 10, 25, 50, 100 and 200 μM. The symbols are: **OX**-1, ●; **OX**-6, □; **OX**-7, ▲. All tests were performed in quadruplicate. The data represent the mean ± S.E.M.

Table 2
IC_{50} values for the most active compounds against PTP-1B.

Compound	IC_{50} (μM)
OX-1	11.0 ± 1.8
OX-6	10.1 ± 0.4
OX-7	8.7 ± 0.3

The data represent the IC_{50} value ± S.E.M.
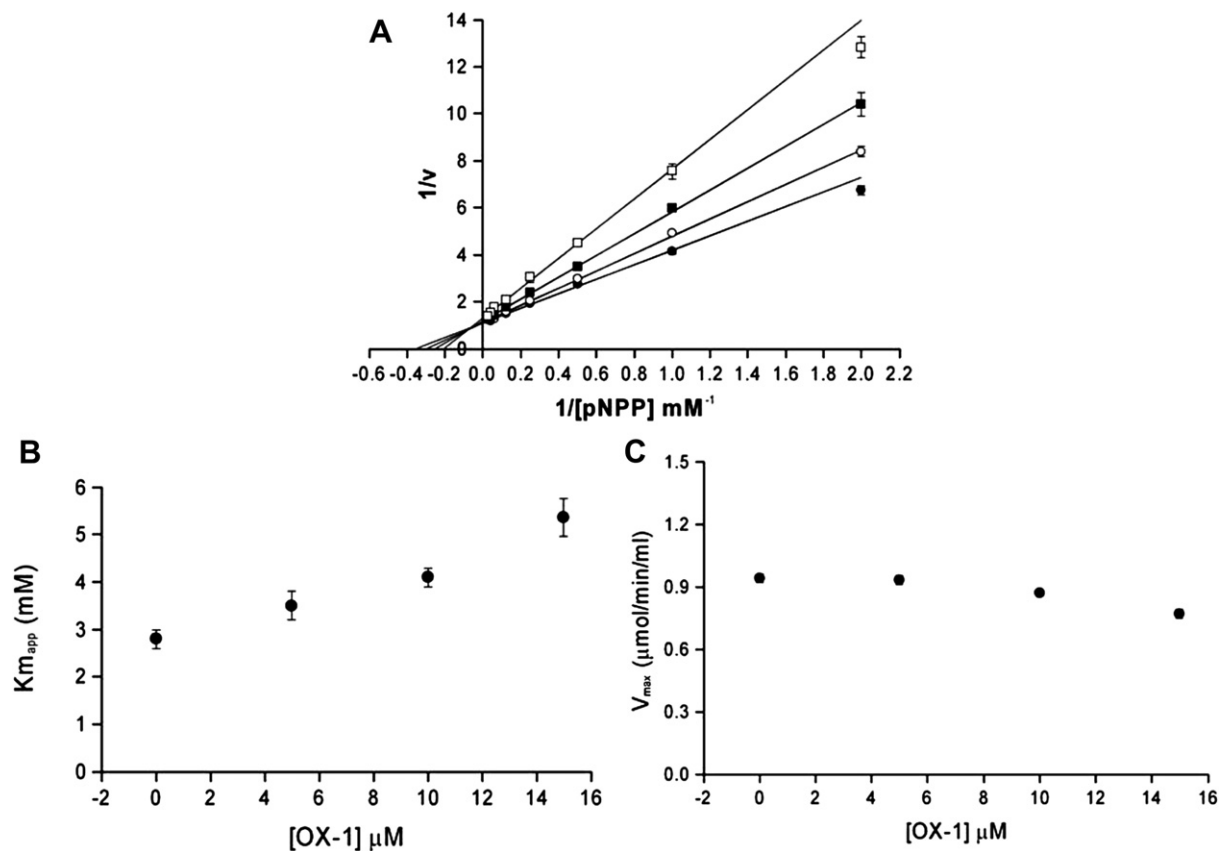
Fig. 6. [A] Double reciprocal plot of **OX-1** (1/v versus 1/[S]). The concentrations of inhibitor used were: 0 μM, ●; 5 μM, ○; 10 μM, ■; 15 μM, □. All tests were performed in quadruplicate. Dependence of main kinetic parameters K_m [B] and V_{max} [C] from the concentration of compound **OX-1**. The data represent the K_m or V_{max} values ± S.E.M.
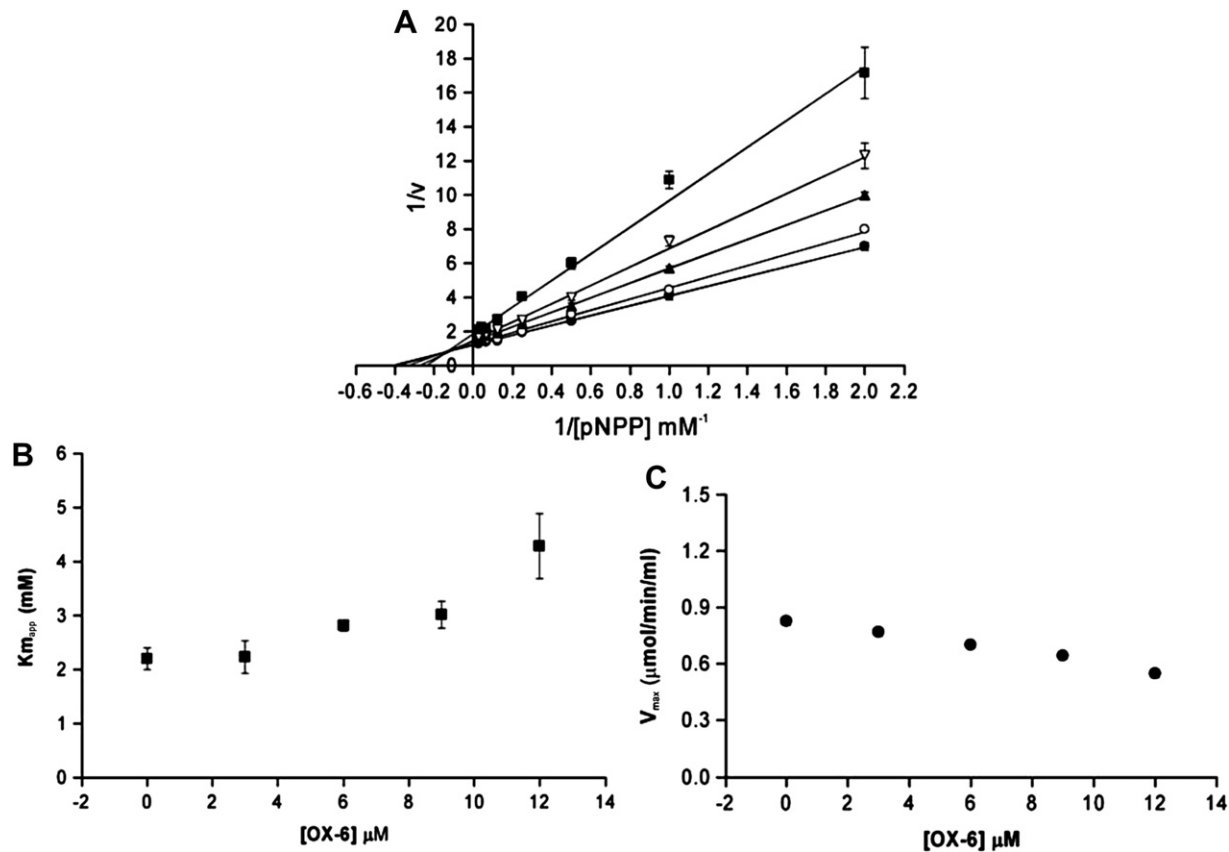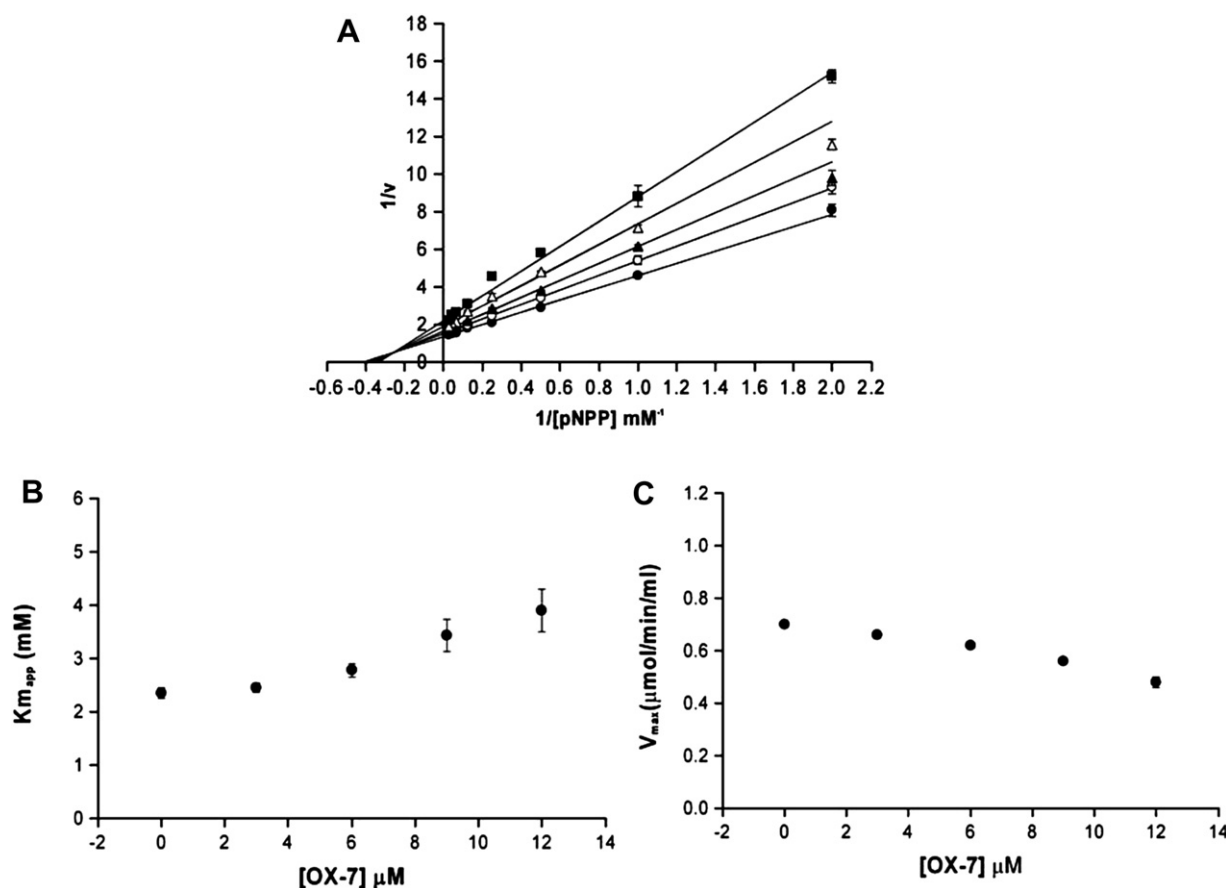

Fig. 7. [A] Compound **OX-6**: double reciprocal plot (1/v versus 1/[S]). The concentrations of inhibitor used were: 0 μM, ●; 3 μM, ○; 6 μM, ▲; 9 μM, ▽; 12 μM, ■. All tests were performed in quadruplicate. Dependence of main kinetic parameters K_m [B] and V_{max} [C] from the concentration of compound **OX-6**. The data represent the K_m or V_{max} values ± S.E.M.

Fig. 8. [A] Compound **OX-7**: double reciprocal plot (1/v versus 1/[S]). The concentrations of inhibitor used were: 0 μM, ●; 3 μM, ○ 6 μM, ▲; 9 μM, ▽; 12 μM, ■. All tests were performed in quadruplicate. Dependence of main kinetic parameters K_m [B] and V_{max} [C] from the concentration of compound **OX-7**. The data represent the K_m or V_{max} values ± S.E.M.

Table 4 shows the predicted binding free energy of the co-crystal ligand and benzothiazole derivatives along with their corresponding experimental K_i values. In general, the binding energies are similar. This result is in line with the comparable experimental activity of the three compounds. In addition, all compounds showed better affinities than the crystal ligand.

Fig. 10 shows the binding mode of **OX-1**. It has a similar binding as the co-crystal ligand and both form a similar hydrogen bond network with the catalytic site.

Fig. 11 shows a comparison of the binding mode of the three most active compounds with 6-(oxalyl-amino)-1*H*-indole-5-carboxilic acid. The figures clearly show that the three benzothiazole derivatives have the same binding mode. In addition, all three docked benzothiazole derivatives share the same binding pattern and pharmacophoric interactions as the co-crystal ligand of PTP-1B (1C83). It is notable the three-dimensional similarity of the binding models of the benzothiazole derivatives and 6-(oxalyl-amino)-1*H*-indole-5-carboxilic acid.

Fig. 12 depicts the 2D interactions maps of the 6-(oxalyl-amino)-1*H*-indole-5-carboxilic acid and **OX-1**. A three-dimensional comparison of the binding conformation of the co-crystal ligand and docked **OX-1** is also shown. Hydrogen bond network is conserved by **OX-1** and analogs, with Gly220, Arg221, Asp181, Ser216. As compared to the crystal ligand, **OX-1** and analogs lack of two important hydrogen bonds with Lys120 and Gln262. These considerations could be taken into account for designing new compounds. Interestingly, Asp181, Cys215 and Arg221 are catalytic residues [9]. According to the models predicted by Autodock4, the studied benzothiazole derivatives bind into the catalytic site of PTP-1B.

2.4. In vivo hypoglycemic activity

Compounds **OX-1** and **OX-6** were evaluated for *in vivo* hypoglycemic activity using a normoglycemic rats. Glibenclamide was taken as positive control [7]. The hypoglycemic activity of both
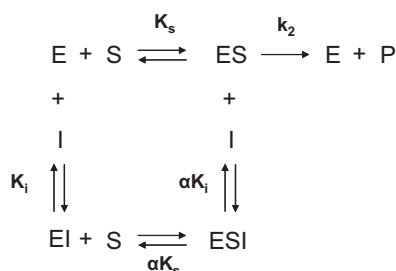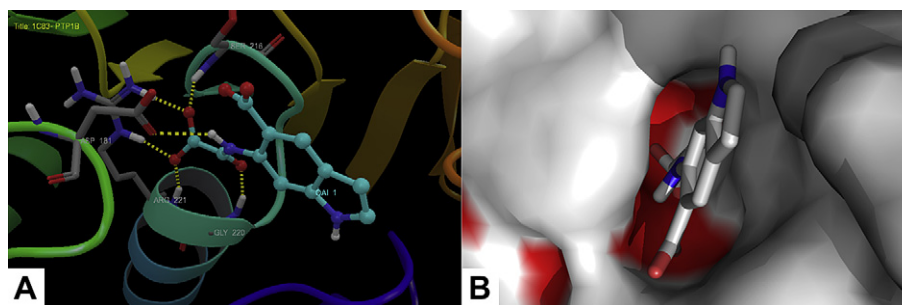

Scheme 1. Linear mixed-type inhibition.

Table 3
The inhibition constants for compounds **OX-1**, **OX-6**, and **OX-7**.

Compound	K_i (μM)	α	Inhibition type
OX-1	6.2 ± 0.7	4.5	Linear mixed-type
OX-6	7.9 ± 0.6	3.8	Linear mixed-type
OX-7	7.9 ± 0.6	1.8	Linear mixed-type

Data represent K_i values ± S.E.M.

Fig. 9. [A] Binding mode of the co-crystal ligand with PTP-1B showing an extensive hydrogen bonds network. Hydrogen bonds are depicted with yellow dashes. [B] Catalytic binding site of PTB-1B. Surface in red shows the residues (Asp181, Ser216, Gly220 and Arg221) that participate in the hydrogen bond network. (For interpretation of the references to color in this figure legend, the reader is referred to the web version of this article.)

Table 4
Docking results of the co-crystal ligand and benzothiazole derivatives into the catalytic site of PTP-1B.

Compound	Binding energy ΔG (Kcal/mol)	Experimental inhibition constant K_i (µM)
Co-crystal ligand	−6.01	14.0 [8]
OX-1	−6.37	6.2
OX-6	−6.35	7.9
OX-7	−6.01	7.9

compounds was determined using a 100 mg/kg single dose. Compound **OX**-1 demonstrated significant hypoglycemic activity, by lowering glycemia ranging from 26% to 37%. The effect was consistent during the first 5 h of experiment (Fig. 13). Compound **OX**-6 showed similar effects than glibenclamide during the first 3 h, lowering the glycemia until 30%. The most pronounced effect of both compounds was observed during the first 3–5 h of post-intragastric administration.
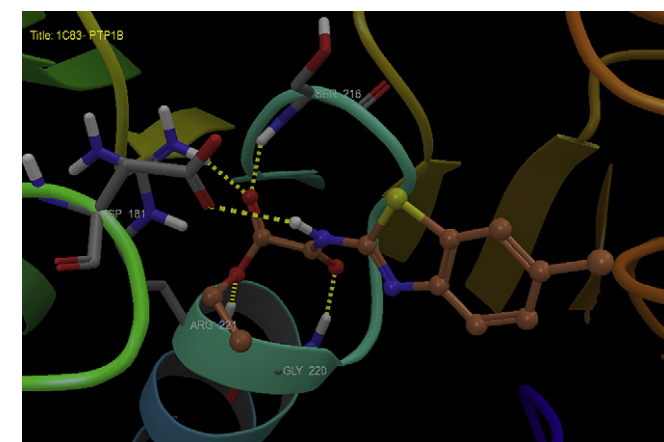
2.5. Oral glucose tolerance test

Compounds **OX**-1 and **OX**-6 were tested in glucose-fed normal rats, and they significantly prevent the rise of blood glucose (more than 20%) when compared with control of glucose-fed normal rats, repaglinide and glibenclamide (Fig. 14). Both compounds significantly diminish hyperglycemic curve induced by overdose of glucose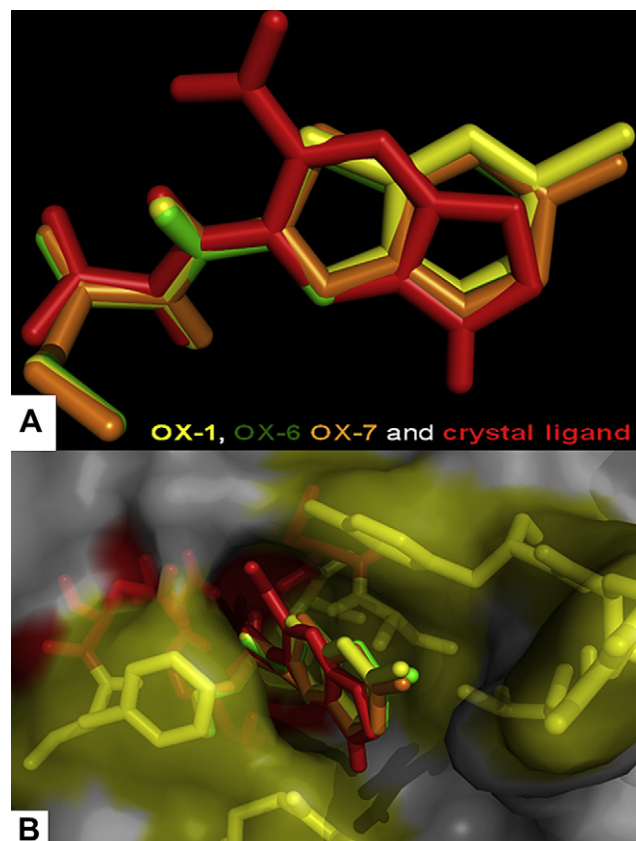 (2 g/kg). This effect is similar to that exercised by glibenclamide in both normoglycemic models, and indicate that exerts a hypoglycemic effect of equal potency and efficacy that repaglinide, confirming the hypoglycemic effects observed in the acute normoglycemic model.

3. Conclusion

We report the synthesis of nine ethyl 2-(6-substituted benzo[d] thiazol-2-ylamino)-2-oxoacetate derivatives which were obtained with modest yields, and evaluated these compounds for their protein tyrosine phosphatase 1B inhibitory activity. Several

Fig. 11. [A] Docked benzothiazole derivatives and co-crystal ligand. They represent the lowest energy conformation estimated by Autodock4. [B] Docked benzothiazole derivatives into the catalytic binding site. Residues forming hydrogen bonds in red: Asp181, Ser216, Gly220 and Arg221. Residues making van der Waals contacts in yellow: Tyr46, Arg47, Val49 and Phe182. (For interpretation of the references to color in this figure legend, the reader is referred to the web version of this article.)

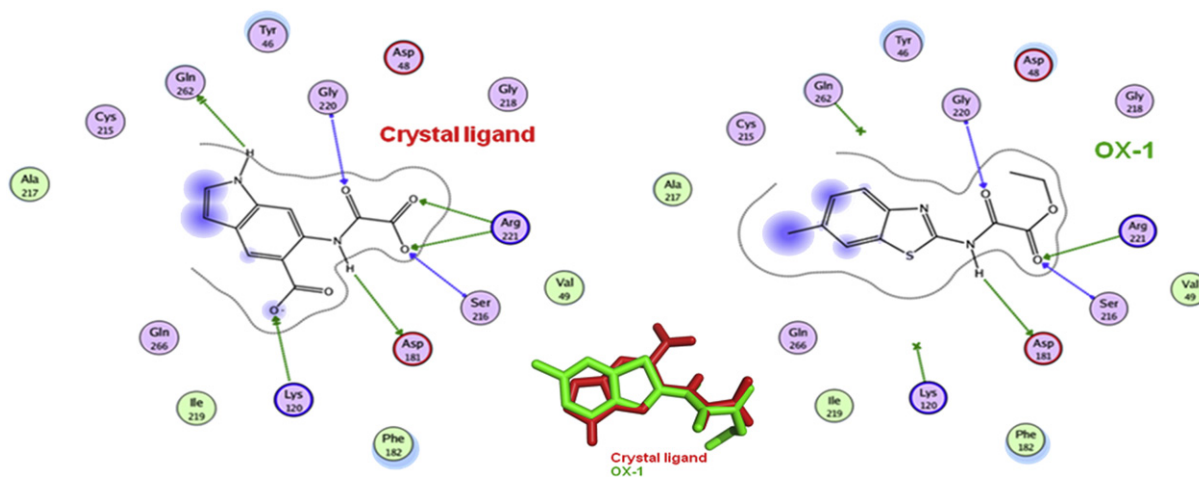**Fig. 10.** Binding model of **OX**-1 in the catalytic site of PTP-1B. Hydrogen bonds are depicted with yellow dashes. (For interpretation of the references to color in this figure legend, the reader is referred to the web version of this article.)

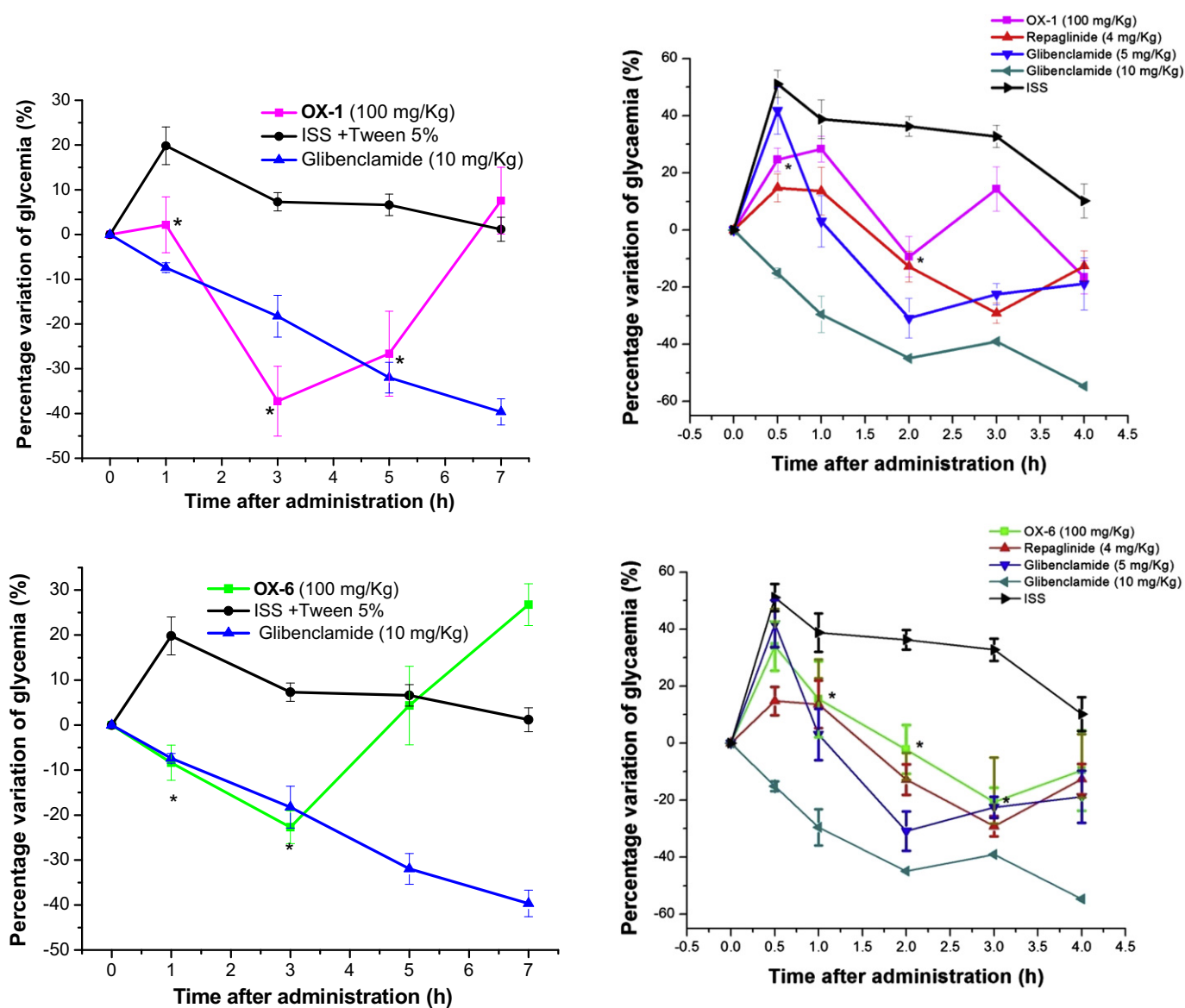**Fig. 12.** 2D dimensional interaction maps of the crystal ligand and **OX**-**1**.

Fig. 13. Effect of a single dose of **OX-1** and **OX-6** (100 mg/kg; intragastric, $n = 5$) in normoglycemic rats. ISS: Isotonic saline solution. $^*p < 0.05$ versus ISS group.

Fig. 14. Oral glucose tolerance test. Effect of a single dose of **OX-1** and **OX-6** (100 mg/kg; intragastric route, $n = 5$) in normoglycemic rats. ISS: Isotonic saline solution. $^*p < 0.05$ versus ISS group.

compounds of this series have shown significant PTP-1B inhibitory activity in the low micro-molar range. Compounds **OX-1**, **6** and **7** exhibited the most promising activity as reversible and non-slow binding mixed-type inhibitors of PTP-1B. Docking results indicate potential hydrogen bond interactions between the oxamate group in all compounds and the catalytic amino acid residues Arg221 and Ser216. Compounds **OX-1**, **6** and **7** were two to four-times more active than previously benzothiazole inhibitors synthesized by our group [7].

The *in vivo* hypoglycemic activities of these compounds make them a suitable leads to develop new chemical entities for potential use in the treatment of diabetes.

4. Experimental

4.1. Chemistry

Melting points were determined on an EZ-Melt MPA120 automated melting point apparatus from Stanford Research Systems and are uncorrected. Reactions were monitored by TLC on 0.2 mm precoated silica gel 60 F254 plates (E. Merck). ^{1}H NMR spectra were recorded on a Varian Oxford (400 MHz) and ^{13}C NMR (100 MHz) instrument. Chemical shifts are given in ppm relative to tetramethylsilane (Me$_4$Si, $\delta = 0$) in DMSO-d_6; J values are given in Hz. The following abbreviations are used: s, singlet; d, doublet; q, quartet; dd, doublet of doublet; t, triplet; m, multiplet; bs, broad signal. MS were recorded on a JEOL JMS-700 spectrometer by Fast Atom Bombarded [FAB (+)]. Starting materials were commercially available from Aldrich and used without purification.

4.1.1. General method of synthesis of ethyl 2-(6-substituted benzo [d]thiazol-2-ylamino)-2-oxoacetates (**1–8**)

To a solution of 2-amino-6-substituted benzo[d]thiazole (0.0015 mol) in dichloromethane was added triethylamine (1.2 equiv.). The reaction mixture was stirred at 5 °C for 15 min. After that, a solution of ethyl chlorooxoacetate (0.0018 mol, 1.2 equiv.) was added droopingly. The reaction mixture was stirred at room temperature for 9–32 h. After complete conversion as indicated by TLC, the solvent was removed *in vacuo*, the residue was neutralized with saturated NaHCO$_3$ solution, and the aqueous layer was extracted with ethyl acetate (3 × 15 mL), washed with water (3 × 20 mL), and dried over anhydrous Na$_2$SO$_4$. The solvent was evaporated *in vacuo* and the precipitated solids were recrystalized from a mixture of ethanol:acetone or purified by column chromatography.

4.1.1.1. Ethyl 2-(6-methylbenzo[d]thiazol-2-ylamino)-2-oxoacetate (**OX-1**). Yield: 52%, mp: 163–165 °C. ^{1}H NMR (400 MHz, DMSO-d_6) δ: 7.69 (1H, s, H-7), 7.65 (1H, d, J_o = 8 Hz, H-4), 7.25 (^{1}H, dd, J_o = 7.5 Hz, J_m = 1 Hz, H-5), 4.29 (2H, q, CH$_2$), 2.38 (3H, s, CH$_3$), 1.2 (3H, t, CH$_3$) ppm; ^{13}C NMR (100 MHz, DMSO-d_6) δ: 160.2 (C-2′), 158.4 (C-1′), 158.1 (C-2), 146.6 (C-3a), 134.9 (C-7a), 132.6 (C-6), 129.0 (C-5), 122.6 (C-7), 121.3 (C-4), 63.9 (CH$_2$), 22.2 (CH$_3$) 15.0 (CH$_3$) ppm; MS/FAB$^+$: m/z 265 (M + H$^+$). HRMS (FAB$^+$): m/z 265.07062 [M + H]$^+$ (Calculated for C$_{12}$H$_{12}$N$_2$O$_3$SH$^+$ 265.0647).

4.1.1.2. Ethyl 2-(benzo[d]thiazol-2-ylamino)-2-oxoacetate (**OX-2**). Yield: 49%, mp: 187–188 °C. ^{1}H NMR (400 MHz, DMSO-d_6) δ: 8.03 (1H, d, J_o = 7.88 Hz, H-7), 7.84 (1H, d, J_o = 8.4 Hz, H-4), 7.47 (1H, m, J_o = 7.6 Hz, J_o = 7.6 Hz, J_m = 1.1 Hz, H-6), 7.36 (1H, m, J_o = 7.3 Hz, J_o = 7.3 Hz, J_m = 1.1 Hz, H-5), 4.32 (2H, q, H-3′), 1.32 (3H, *t*, H-4′) ppm; ^{13}C NMR (100 MHz, DMSO-d_6) δ: 159.1 (C-2′), 157.9 (C-1′), 157.4 (C-2), 147.5 (C-3a), 131.4 (C-7a), 126.5 (C-6), 124.2 (C-5), 122.0 (C-7), 120.5 (C-4), 62.7 (CH$_2$), 13.7 (CH$_3$) ppm;

MS/FAB$^+$: m/z 251 (M + H$^+$). HRMS (FAB$^+$): m/z 251.0483 [M + H]$^+$ (Calculated for C$_{11}$H$_{10}$N$_2$O$_3$SH$^+$ 251.0490).

4.1.1.3. Ethyl 2-(6-methoxybenzo[d]thiazol-2-ylamino)-2-oxoacetate (**OX-3**). Yield: 45%, mp: 182–184 °C. ^{1}H NMR (400 MHz, DMSO-d_6) δ: 7.69 (1H, d, J_o = 8.8 Hz, H-4), 7.61 (1H, d, J_m = 2.4 Hz, H-7), 7.06 (1H, dd, J_m = 2.4 Hz, J_m = 2.4 Hz, J_o = 8.8 Hz, H-5), 4.31 (2H, q, CH$_2$), 3.80 (3H, s, CH$_3$O), 1.31 (3H, t, CH$_3$) ppm; ^{13}C NMR (100 MHz, DMSO-d_6) δ: 159.0 (C-2′), 156.8 (C-1′), 156.4 (C-2), 155.4 (C-6), 141.8 (C-3a), 132.8 (C-7a) 121.2 (C-5), 115.3 (C-7), 104.7 (C-4), 62.6 (CH$_2$), 55.6 (CH$_3$O) 13.7 (CH$_3$) ppm; MS/FAB$^+$: m/z 281 (M + H$^+$). HRMS (FAB$^+$): m/z 281.0587 [M + H]$^+$ (Calculated for C$_{12}$H$_{12}$N$_2$O$_4$SH$^+$ 281.0596).

4.1.1.4. Ethyl 2-(6-ethoxybenzo[d]thiazol-2-ylamino)-2-oxoacetate (**OX-4**). Yield: 44%, mp: 176–178 °C. ^{1}H NMR (400 MHz, DMSO-d_6) δ: 7.68 (1H, d, J_o = 8.8 Hz, H-4), 7.59 (1H, d, J_m = 2.2 Hz, H-7), 7.05 (1H, dd, J_m = 2.2 Hz, J_m = 2, J_o = 8.8 Hz, H-5), 4.31 (2H, q, CH$_2$), 4.06 (2H, q, CH$_2$), 1.34 (3H, t, CH$_3$), 1.31 (3H, t, CH$_3$) ppm.; ^{13}C NMR (100 MHz, DMSO-d_6) δ: 168.4 (C-2′), 159.0 (C-1′), 156.8 (C-2), 155.6 (C-6), 141.7 (C-3a), 132.8 (C-7a) 121.2 (C-5), 115.6 (C-7), 105.3 (C-4), 63.6 (CH$_2$), 62.6 (CH$_2$), 14.7 (CH$_3$) 13.7 (CH$_3$) ppm; MS/FAB$^+$: m/z 295 (M + H$^+$). HRMS (FAB$^+$): m/z 295.0770 [M + H]$^+$ (Calculated for C$_{13}$H$_{14}$N$_2$O$_4$SH$^+$ 295.0753).

4.1.1.5. Ethyl 2-{6-(methylsulfonyl)benzo[d]thiazol-2-ylamino}-2-oxoacetate (**OX-5**). Yield: 98%, mp: 209–212 °C. ^{1}H NMR (400 MHz, DMSO-d_6) δ: 8.14 (1H, s, H-7), 7.77 (1H, d, J_o = 8 Hz, H-4), 7.46 (1H, dd, J_o = 8 Hz, J_m = 1 Hz, H-5), 4.3 (2H, q, CH$_2$), 2.49 (3H, s, CH$_3$), 1.31 (3H, t, CH$_3$) ppm; ^{13}C NMR (100 MHz, DMSO-d_6) δ: 162.7 (C-2′), 159.7 (C-1′), 158.6 (C-2), 152.6 (C-3a), 137.2 (C-6), 133.2 (C-7a), 126.2 (C-7) 123.5 (C-4), 122.2 (C-5), 64.1 (CH$_2$), 45.1 (CH$_3$), 15.0 (CH$_3$) ppm; MS/FAB$^+$: m/z 329 (M + H$^+$). HRMS (FAB$^+$): m/z 329.0233 [M + H]$^+$ (Calculated for C$_{12}$H$_{12}$N$_2$O$_5$S$_2$H$^+$ 329.0266).

4.1.1.6. Ethyl 2-(6-chlorobenzo[d]thiazol-2-ylamino)-2-oxoacetate (**OX-6**). Yield: 47%, mp: 218–221 °C. ^{1}H NMR (400 MHz, DMSO-d_6) δ: 8.13 (1H, s, H-7), 7.76 (1H, d, J_o = 8.4 Hz, H-4), 7.48 (1H, dd, J_m = 1.2 Hz, J_o = 8.4 Hz, H-5), 4.30 (2H, q, CH$_2$), 1.30 (3H, t, CH$_3$) ppm; ^{13}C NMR (100 MHz, DMSO-d_6) δ: 159.9 (C-2′), 159.5 (C-1′), 158.2 (C-2), 148.0 (C-3a), 134.3 (C-7a), 129.4 (C-5) 127.9 (C-6), 122.9 (C-4), 122.6 (C-7), 64.0 (CH$_2$), 15.08 (CH$_3$) ppm; MS/FAB$^+$: m/z 285 (M + H$^+$). HRMS (FAB$^+$): m/z 285.0091 [M + H]$^+$ (Calculated for C$_{11}$H$_9$ClN$_2$O$_3$SH$^+$ 285.0101).

4.1.1.7. Ethyl 2-(6-fluorobenzo[d]thiazol-2-ylamino)-2-oxoacetate (**OX-7**). Yield: 63%, mp: 214–215 °C. ^{1}H NMR (400 MHz, DMSO-d_6) δ: 7.93 (1H, dd, $J_{m, H-H}$ = 2.6 Hz, $J_{o, H-F}$ = 8.72 Hz, H-7), 7.81 (1H, dd, $J_{o, H-H}$ = 8.92 Hz, $J_{m, H-F}$ = 4.8 Hz, H-4), 7.32 (1H, td, $J_{m, H-H}$ = 2.7 Hz, $J_{o, H-H}$ = 9.12 Hz, $J_{o, H-F}$ = 9.04 Hz, H-5), 4.32 (2H, q, CH$_2$), 1.31 (3H, t, CH$_3$) ppm; ^{13}C NMR (100 MHz, DMSO-d_6) δ: 158.9 (d, J = 239.24 Hz, C-6), 158.93 (C-2′), 157.5 (C-1′), 157.1 (d, J_p = 0.81 Hz, C-3a), 144.8 (C-2), 132.8 (d, J_m = 11.39 Hz, C-7a), 122.0 (d, J_m = 9.05 Hz, C-4), 114.6 (d, J_o = 24.57 Hz, C-7), 108.3 (d, J_o = 26.69 Hz, C-5), 62.7 (CH$_2$), 13.7 (CH$_3$) ppm; MS/FAB$^+$: m/z 269 (M + H$^+$). HRMS (FAB$^+$): m/z 269.0392 [M + H]$^+$ (Calculated for C$_{11}$H$_9$FN$_2$O$_3$SH$^+$ 269.0396).

4.1.1.8. Ethyl 2-(6-nitrobenzo[d]thiazol-2-ylamino)-2-oxoacetate (**OX-8**). Yield: 80%, mp: 255 °C (dec). ^{1}H NMR (400 MHz, DMSO-d_6) δ: 9.03 (1H, s, H-7), 8.24 (1H, dd, J_o = 8.8 Hz, J_m = 1 Hz, H-5), 7.89 (1H, d, J_o = 8.8 Hz, H-4), 4.30 (2H, t, CH$_2$) 1.31 (3H, t, CH$_3$) ppm; ^{1}C NMR (100 MHz, DMSO-d_6) δ: 162.8 (C-2′), 158.3 (C-1′), 157.2 (C-2), 152.6 (C-3a), 143.2 (C-6), 132.1 (C-7a) 121.7 (C-4),

120.8 (C-7), 119.1 (C-5), 62.9 (CH$_2$), 13.7 (CH$_3$) ppm; MS/FAB$^+$: m/z 296 (M + H$^+$). HRMS (FAB$^+$): m/z 296.0393 [M + H]$^+$ (Calculated for C$_{11}$H$_9$N$_3$O$_5$SH$^+$ 296.0341).

4.1.1.9. Ethyl 2-(6-aminobenzo[d]thiazol-2-ylamino)-2-oxoacetate (**OX-9**). Yield: 90%, mp: 290 °C (dec). ^{1}H NMR (400 MHz, DMSO-d_6) δ: 6.84 (1H, s, H-7), 6.60 (1H, dd, J_o = 8.8 Hz, J_m = 1 Hz, H-5), 7.59 (1H, d, J_o = 8.8 Hz, H-4), 4.32 (2H, t, CH$_2$) 1.34 (3H, t, CH$_3$) ppm; ^{13}C NMR (100 MHz, DMSO-d_6) δ: 158.2 (C-2′), 156.5 (C-1′), 150.4 (C-2), 148.4 (C-3a), 145.7 (C-6), 127.1 (C-7a) 122.1 (C-4), 113.8 (C-5), 103.8 (C-7), 63.2 (CH$_2$), 14.7 (CH$_3$) ppm; MS/FAB$^+$: m/z 266 (M + H$^+$). HRMS (FAB$^+$): m/z 266.0578 [M + H]$^+$ (Calculated for C$_{11}$H$_{11}$N$_3$O$_3$SH$^+$ 266.0593).

4.2. Biological assays

4.2.1. PTP-1B expression and purification

All experiments were conducted using human recombinant PTP-1B. Briefly, the complete sequence of PTP-1B was cloned in the pGEX-2T bacterial expression vector downstream the GST sequence. This vector was used to transform *E. coli* TB1 strain cells. The recombinant fusion protein was purified from bacterial lysate using a single-step affinity chromatography. The solution containing purified fusion protein was treated with thrombin for 3 h at 37 °C. Then the PTP-1B was purified from GST and thrombin by gel filtration on a Superdex G75 column. The purity of PTP-1B preparation was assessed by SDS–polyacrylamide gel electrophoresis.

4.2.2. Enzyme assays [10]

All assays were carried out at 37 °C. The substrate (*p*-nitrophenylphosphate) was dissolved in 0.075 M of β,β-dimethylglutarate buffer pH 7.0, containing 1 mM EDTA and 1 mM dithiothreitol. The final volume was 1 mL. The reactions were initiated by adding aliquots of the enzyme (0.16 μg for each test), and stopped at appropriate times with 4 mL of 1 M KOH. The released *p*-nitrophenol was determined by reading the absorbance at 400 nm (ε = 18,000 M^{-1} cm^{-1}). The main kinetic parameters (K_m and V_{max}) were determined by measuring the initial rates using eight different substrate concentrations in the 0.5–40 mM range. Experimental data were analyzed using the Michaelis–Menten equation and a nonlinear fitting program (FigSys).

To evaluate the inhibition power of compounds **OX-1**, **OX-6**, and **OX-7** we calculated the IC$_{50}$ value using a fixed substrate concentration corresponding to the K_m of enzyme and varying inhibitor concentrations. The IC$_{50}$ value was calculated by fitting experimental data with a non-nonlinear fitting program (FigSys, Biosoft, UK), using the equation:

$$y = \frac{\text{Max} - \text{Min}}{1 + \left(\frac{x}{\text{IC}_{50}}\right)^{\text{slope}}} + \text{Min}$$

where "*y*" is vi/vo, i.e. the ratio between the activity measure in the presence of the inhibitor (vi) and the activity of the control without the inhibitor (vo). The parameter "*x*" is the inhibitor concentration.

4.2.3. Animals

Male Wistar rats weighing 200–250 g body weight were housed at standard laboratory conditions and fed with a rodent pellet diet and water *ad libitum*. They were maintained at room temperature and at a photoperiod of 12 h day/night cycle. Animals described as fasted were deprived of food for 18 h but had free access to water. All animal procedures were conducted in accordance with our Federal Regulations for Animal Experimentation and Care (SAGARPA, NOM-062-ZOO-1999, México), and approved by the Institutional Animal Care and Use Committee based on US National Institute of Health publication (No. 85-23, revised 1985).

4.2.4. In vivo hypoglycemic assay

Animals were divided into groups of five animals each (n = 5). Experimental groups were orally treated with a single dose (100 mg/kg body weight) of suspension of the compounds **OX-1**, **OX-6**, and **OX-7** (prepared in 5% Tween 80). Control group animals were also fed with 5% Tween 80. Glibenclamide (10 mg/kg) was used as hypoglycemic reference drug. Blood samples were collected from the caudal vein at 0, 1, 3, 5, and 7 h after vehicle, sample and drug administration. Blood glucose concentration was estimated by enzymatic glucose oxidase method using a commercial glucometer (Accutrend GCT, Roche®). The percentage variation of glycemia for each group was calculated in relation to initial (0 h) level, according to: %Variation of glycemia = [(G_x − G_0)/G_0] × 100, where G_0 were initial glycemia values and G_x were the glycemia values at +1, +3, +5 and +7 h, respectively. All values were expressed as mean ± S.E.M. Statistical significance was estimated by analysis of variance (ANOVA), p < 0.05 implies significance.

4.2.5. Oral glucose tolerance test [11]

After a food overnight deprivation of 18 h, normoglycemic rats (n = 5) were subjected to an oral glucose tolerance test (OGTT) to investigate the short-term hypoglycemic effect of the compounds.

Compounds **OX-1** and **OX-6** (100 mg/kg), vehicle, acarbose (10 mg/kg), repaglinide (4 mg/kg) and glibenclamide (5 and 10 mg/kg) were administered to rats in the equal volume of suspension, and 10 min after received a single dose of glucose (2 g/kg) by de same route. Blood samples were collected from the tail tip at 0 (before oral administration), 0.5, 1, 2, 3 and 4 h after vehicle, positive controls and samples administration. Blood glucose concentration was estimated as described.

4.2.6. Docking

Molecular Operating Environment (MOE) 2009.10 was used for ligand and protein preparation, and molecular structure viewing. The crystal structure was obtained from the PDB with the accession code 1C83 [8]. Docking calculations were conducted with Auto-Dock, version 4.0 [12]. In short, AutoDock performs an automated docking of the ligand with user-specified dihedral flexibility within a protein rigid binding site. The program performs several runs in each docking experiment. Each run provides one predicted binding mode. All water molecules and 6-(oxalyl-amino)-1*H*-indole-5-carboxylic acid (crystallographic ligand) were removed from the crystallographic structure and all hydrogen atoms were added. For all ligands and protein, Gasteiger charges were assigned and nonpolar hydrogen atoms were merged. All torsions were allowed to rotate during docking. The auxiliary program AutoGrid generated the grid maps. Each grid was centered at the crystallographic coordinates of the crystallographic compound. The grid dimensions were 22.12 × 22.12 × 22.12 Å^3 with points separated by 0.375 Å. Lennard–Jones parameters 12−10 and 12−6, supplied with the program, were used for modeling H-bonds and Van der Waals interactions, respectively. The Lamarckian genetic algorithm was applied for the search using default parameters. The number of docking runs was 100. After docking, the 100 solutions were clustered into groups with RMS lower than 1.0 Å. The clusters were ranked by the lowest energy representative of each cluster. In order to describe the ligand-binding pocket interactions, the top ranked binding mode found by AutoDock in complex with the binding pocket of PTP-1B was subject to full energy minimization using the MMFF94 force field implemented in MOE until the gradient 0.05 was reached. PyMOL 1.0 [13] was used to generate the molecular surface of docking models.

Acknowledgments

Appendix A. Supplementary data

Supplementary data related to this article can be found online at doi:10.1016/j.ejmech.2012.04.025.

References

[1] L. Gang, Protein tyrosine phosphatase 1B inhibition: opportunities and challenges, Curr. Med. Chem. 10 (2003) 1407–1421.

[2] S. Gupta, G. Pandey, N. Rahuja, A.K. Srivastava, A.K. Saxena, Design, synthesis and docking studies on phenoxy-3-piperazin-1-yl-propan-2-ol derivatives as protein tyrosine phosphatase 1B inhibitors, Bioorg. Med. Chem. Lett. 20 (2010) 5732–5734.

[3] C. Ramachandran, B.P. Kennedy, Protein tyrosine phosphatase 1B: a novel target for type 2 diabetes and obesity, Curr. Top. Med. Chem. 3 (2003) 749–757.

[4] A.P. Combs, Recent advances in the discovery of competitive protein tyrosine phosphatase 1B inhibitors for the treatment of diabetes, obesity, and cancer, J. Med. Chem. 53 (2010) 2333–2344.

[5] S. Zhang, Z.Y. Zhang, PTP1B as a drug target: recent developments in PTP1B inhibitor discovery, Drug Discov. Today 12 (2007) 373–381.

[6] R. Sarabu, J. Tilley, Recent advances in therapeutic approaches to type 2 diabetes, Annu. Rep. Med. Chem. 40 (2005) 167–181.

[7] G. Navarrete-Vazquez, P. Paoli, I. León-Rivera, R. Villalobos-Molina, J.L. Medina-Franco, R. Ortiz-Andrade, S. Estrada-Soto, G. Camici, D. Diaz-Coutiño, I. Gallardo-Ortiz, K. Martinez-Mayorga, H. Moreno-Díaz, Synthesis, in vitro and computational studies of protein tyrosine phosphatase 1B inhibition of a small library of 2-arylsulfonylaminobenzothiazoles with antihyperglycemic activity, Bioorg. Med. Chem. 17 (2009) 3332–3341.

[8] H.S. Andersen, L.F. Iversen, C.B. Jeppesen, S. Branner, K. Norris, H.B. Rasmussen, K.B. Møller, N.P. Møller, 2-(Oxalylamino)-benzoic acid is a general, competitive inhibitor of protein-tyrosine phosphatases, J. Biol. Chem. 275 (2000) 7101–7108.

[9] L. Bialy, H. Waldmann, Inhibitors of protein tyrosine phosphatases: next-generation drugs? Angew. Chem. Int. Ed. 44 (2005) 3814–3839.

[10] R. Maccari, P. Paoli, R. Ottanà, M. Jacomelli, R. Ciurleo, G. Manao, T. Steindl, T. Langer, M.G. Vigorita, G. Camici, 5-Arylidene-2, 4-thiazolidinediones as inhibitors of protein tyrosine phosphatases, Bioorg. Med. Chem. 15 (2007) 5137–5149.

[11] R. Ortiz-Andrade, J.C. Sachez-Sagado, G. Navarrete-Vázquez, S.P. Webster, M. Binnie, S. García-Jiménez, I. León-Rivera, P. Cigarroa-Vázquez, R. Villaobos-Molina, S. Estrada-Soto, Antidiabetic and toxicologial evaluations of naringenin in normoglycemic and NIDMM rat models and its implications on extra-pancreatic glucose regulation, Diabetes Obes. Metab. 10 (2008) 1097–1104.

[12] R. Huey, G.M. Morris, A.J. Olson, D.S. Goodsell, A semiempirical free energy force field with charge-based desolvation, J. Comput. Chem. 28 (2007) 1145–1152.

[13] W.L. DeLano, The PyMOL Molecular Graphics System. DeLano Scientific LLC, San Carlos, CA, USA. Available at: http://www.pymol.org.